A Parallel Adaptive Finite Element Method for Modeling a Deformable Droplet Travelling in Air

Li Luo, Xiao-Chuan Cai, and David E. Keyes

1 Introduction

Violent respiratory events such as coughing and sneezing can contribute to the transmission of infectious diseases from host to host. The dynamics of droplet transfer between individuals and the range of contamination are extremely complex and remain unclear [3]. Studying the fluid dynamics of pathogen-laden droplets is critically important to controlling the pandemic.

Fluid dynamics studies of violent ejections are presented in [1, 4]. These studies focus on analytical modeling of the puff evolution or the transport of inertial spherical droplets to understand the available quantitative relationships. CFD simulation has been conducted to investigate the dispersion of airborne particles by using a Lagrangian-based model for particle motion [10] or by coupling the Navier-Stokes equations with an additional transport equation for a scalar concentration field [9]. Although the transport of particles in a crowd are detailed in these studies, the travelling process of an individual droplet and its dynamics subject to the combined effect of size, gravitational settling, surface tension, and aerodynamic forces are not given particular attention. To address these issues, incorporating multi-phase flow physics in the modeling is necessary [3].

In this work, we study the process of a deformable droplet travelling over a long distance based on two-phase flow simulation, with focus on the two-way coupling between the droplet dynamics and the ambient airflow through advection and surface tension, in order to provide some numerical understanding of the transmission of

Li Luo
Faculty of Science and Technology, University of Macau, Macau, China, e-mail: liluo@um.edu.mo

Xiao-Chuan Cai
Faculty of Science and Technology, University of Macau, Macau, China, e-mail: xccai@um.edu.mo

David E. Keyes
Extreme Computing Research Center, King Abdullah University of Science and Technology, Thuwal, Saudi Arabia, e-mail: david.keyes@kaust.edu.sa

covid19. A phase-field model consisting of the coupled Cahn-Hilliard-Navier-Stokes equations with appropriate boundary conditions is used to describe the two-phase flow. Due to the vast difference between the size of the droplets and the long trajectories they travel (over 1000 times), the problem is computationally very expensive and rarely addressed by previous studies of phase-field methods. To tackle this issue, we develop an efficient adaptive finite element method based on a posterior error estimate to refine elements near the interface, while using coarse elements elsewhere to save computation. In the numerical experiments, we are mainly concerned with: 1) the influence of the droplet size on its shape dynamics and travelling path; 2) the influence of the droplet motion on the surrounding airflow; and 3) the lift and drag forces acting on the droplet through the trajectory.

2 A mathematical model based on the Cahn-Hilliard-Navier-Stokes equations

In a bounded domain $\Omega \subset \mathbb{R}^d$ $(d = 2, 3)$, the system of two immiscible incompressible fluids can be described by the coupled Cahn-Hilliard-Navier-Stokes equations:

$$\frac{\partial \varphi}{\partial t} + \mathbf{u} \cdot \nabla \varphi = L_d \Delta \mu, \qquad \mu = -\epsilon \Delta \varphi - \frac{\varphi}{\epsilon} + \frac{\varphi^3}{\epsilon}, \tag{1}$$

$$Re\rho \left(\frac{\partial \mathbf{u}}{\partial t} + (\mathbf{u} \cdot \nabla)\mathbf{u} \right) = \nabla \cdot \boldsymbol{\sigma} - \frac{Re\rho}{Fr^2} \mathbf{e}_g, \qquad \nabla \cdot \mathbf{u} = 0. \tag{2}$$

Here, a phase field variable φ is introduced to describe the transition between the two homogeneous equilibrium phases $\varphi_\pm = \pm 1$. μ is the chemical potential, ϵ is the ratio between the interface thickness and the characteristic length. $\boldsymbol{\sigma} = -p\mathbf{I} + \eta D(\mathbf{u}) - B\epsilon(\nabla\varphi \otimes \nabla\varphi)$ is the total stress tensor, where p is the pressure, $\mathbf{u}$ is the fluid velocity field, and $D(\mathbf{u}) = \nabla\mathbf{u} + (\nabla\mathbf{u})^T$ is the rate of strain tensor. The term $\epsilon(\nabla\varphi \otimes \nabla\varphi)$ represents the capillary force. The mass density ρ and the dynamic viscosity η are interpolation functions of φ between fluid 1 and fluid 2, i.e. $\rho = \frac{1+\varphi}{2} + \lambda_\rho \frac{1-\varphi}{2}$, $\eta = \frac{1+\varphi}{2} + \lambda_\eta \frac{1-\varphi}{2}$, where $\lambda_\rho = \rho_2/\rho_1$ is the ratio of density between the two fluids and $\lambda_\eta = \eta_2/\eta_1$ is the ratio of viscosity. $\mathbf{e}_g$ is the unit gravitational vector and Fr is the Froude number. L_d is the phenomenological mobility coefficient, Re is the Reynolds number, and B measures the strength of the capillary force compared to the Newtonian fluid stress.

We assume $\partial\Omega = \Gamma_i \cup \Gamma_o \cup \Gamma_w$, where Γ_i denotes the inflow boundary, Γ_o denotes the outflow boundary, and Γ_w denotes the solid surface. Given functions φ_i and $\mathbf{u}_i$, the boundary conditions on Γ_i are stated as

$$\varphi = \varphi_i, \quad \mu = 0, \quad \mathbf{u} = \mathbf{u}_i, \qquad \text{on } \Gamma_i. \tag{3}$$

On Γ_o, we consider the following outflow boundary conditions [5],

$$\partial_n \varphi = 0, \quad \partial_n \mu = 0, \qquad \text{on } \Gamma_o, \tag{4}$$

$$-(p + BF(\varphi))\mathbf{n} + \eta \mathbf{n} \cdot D(\mathbf{u}) - \frac{Re\rho}{2} |\mathbf{u}|^2 \chi(\mathbf{u} \cdot \mathbf{n})\mathbf{n} = \mathbf{0}, \qquad \text{on } \Gamma_o, \tag{5}$$

where $F(\varphi) = \frac{\epsilon}{2}|\nabla\varphi|^2 + \frac{1}{4\epsilon}(\varphi^2-1)^2$ is the free energy of the two-phase system. $\chi(\mathbf{u}\cdot\mathbf{n}) = \frac{1}{2}\left(1-\tanh\frac{\mathbf{u}\cdot\mathbf{n}}{U\delta}\right)$ is a smoothed step function, where U is a characteristic velocity scale (here $U = 1$), and $\delta > 0$ is a non-dimensional constant that is sufficiently small. As $\delta \to 0$, χ takes a unit value in regions where $\mathbf{u}\cdot\mathbf{n} < 0$ and vanishes elsewhere.

On Γ_w, we consider the generalized Navier boundary conditions [6]:

$$\frac{\partial\varphi}{\partial t} + \mathbf{u}_\tau\cdot\nabla_\tau\varphi = -V_s L(\varphi), \quad \partial_n\mu = 0, \quad \mathbf{u}\cdot\mathbf{n} = 0, \qquad \text{on } \Gamma_w, \tag{6}$$

$$\left((L_s l_s)^{-1}\mathbf{u}_\tau - BL(\varphi)\nabla_\tau\varphi/\eta + \mathbf{n}\cdot D(\mathbf{u})\right)\times\mathbf{n} = \mathbf{0}, \qquad \text{on } \Gamma_w, \tag{7}$$

where $\mathbf{n}$ is the unit outward normal vector and τ is the unit tangential vector of the boundary. $\mathbf{u}_\tau = \mathbf{u} - (\mathbf{n}\cdot\mathbf{u})\mathbf{n}$, $\nabla_\tau = \nabla - (\mathbf{n}\cdot\nabla)\mathbf{n}$. V_s is a phenomenological parameter, $L(\varphi) = \epsilon\partial_n\varphi + \partial\gamma_{wf}(\varphi)/\partial\varphi$, and $\gamma_{wf}(\varphi) = -\frac{\sqrt{2}}{3}\cos\theta_s\sin(\frac{\pi}{2}\varphi)$, where θ_s is the static contact angle. L_s is the slip length of liquid, $l_s = \frac{1+\varphi}{2} + \lambda_{l_s}\frac{1-\varphi}{2}$, and $\lambda_{l_s} = l_2/l_1$.

3 A parallel, semi-implicit solution algorithm based on an adaptive finite element discretization, and an overlapping Schwarz preconditioned GMRES

We apply a second-order semi-implicit time discretization scheme to decouple φ, $\mathbf{u}$, and p at each time step [6]. Specifically, we apply a convex-splitting of the free energy functional and treat the nonlinear term explicitly so that the resulting matrix has constant coefficients. In addition, we consider a pressure-stabilized method to decouple the Navier-Stokes equations into a convection-diffusion equation for velocity and a Poisson equation for pressure. Then, the pressure equation results in a constant matrix and can be solved efficiently.

The resulting decoupled systems are discretized by a finite element method on unstructured meshes. We use P1-P1 finite element spaces for the Cahn-Hilliard equation and P2-P1 for the Navier-Stokes equations. Let T_h be a triangulation of Ω with h be the mesh size of an element T. We denote by φ_h^n, μ_h^n, $\mathbf{u}_h^n$, p_h^n the finite element interpolations of φ, μ, $\mathbf{u}$, p at the nth time step, respectively. In this work, we use the adaptive mesh refinement (AMR) method to accurately capture the phase field variable φ within the thin interface between the two phases. The AMR procedure is performed in an iterative manner. At each adaptive step, we introduce a physics-informed approach to refine the elements repeatedly if they are fully inside the interface region (i.e., $-0.9 \le \varphi_h^{n+1}|_T \le 0.9$) and their sizes are considered to be large (i.e., $\max_{e\in\partial T}|e| > \bar{e}$, where $\bar{e}$ is a given scale). Meanwhile, we merge adjacent elements if they are divided from the same "parent" and their error indicator Θ_T is sufficiently small, i.e.,

$$\Theta_T < \gamma_c \max_{T\in T_h}\{\Theta_T\}, \quad \text{where} \quad \Theta_T = \left(\sum_{e\in\partial T}\int_e \frac{|e|}{24}\left[\frac{\nabla\varphi_h^{n+1}\cdot\mathbf{n}_e}{2}\right]^2 \mathrm{d}e\right)^{\frac{1}{2}}.$$

Here, Θ_T is the gradient jump of φ_h^{n+1} on the interface of adjacent elements [7]. $[\cdot]$ denotes the jump on the element boundary, $\mathbf{n}_e$ is the unit outward normal vector on e, and γ_c is a given parameter. The iteration of refinement and coarsening is stopped when the maximum error indicator $\max_{T \in T_h}\{\Theta_T\} < tol$, where tol is a prescribed tolerance. Combining the above techniques, we present the overall numerical algorithm as follows:

Algorithm 2 A decoupled solution algorithm based on an adaptive finite element method

Set initial values $\varphi_h^0 (= \varphi_h^{-1})$, $\mathbf{u}_h^0 (= \mathbf{u}_h^{-1})$, p_h^0, and $t = 0$.
Loop in time for $n = 0, \cdots$
1 Solve the Cahn-Hilliard system to update φ_h^{n+1} and μ_h^{n+1}.
2 Loop in AMR for $k = 0, \cdots$
(a) Compute Θ_T for all $T \in T_h$, if $\max_{T \in T_h}\{\Theta_T\} < tol$, go to step 3.
(b) Refine the elements repeatedly if $\varphi_h^{n+1}|_T \in [-0.9, 0.9]$ and $\max_{e \in \partial T} |e| > \bar{e}$.
(c) Merge the adjacent elements if each of them yields $\Theta_T < \gamma_c \max_{T \in T_h}\{\Theta_T\}$.
(d) Update φ_h^{n-1}, φ_h^n, $\mathbf{u}_h^{n-1}$, $\mathbf{u}_h^n$, and p_h^n on the new mesh.
(e) Solve the Cahn-Hilliard system to update φ_h^{n+1} and μ_h^{n+1}.
3 Compute ρ_h^{n+1}, η_h^{n+1}, ${l_s}_h^{n+1}$ using φ_h^{n+1}.
4 Solve the velocity system to update $\mathbf{u}_h^{n+1}$.
5 Solve the pressure system to update p_h^{n+1}.
End time loop

For the purpose of efficiency, we perform the AMR method every n_{skip} time steps, and terminate the AMR loop in step 2 when $\max_{T \in T_h}\{\Theta_T\}$ does not decrease any more. Because the matrices arising from the discretization of the Cahn-Hilliard equation and the pressure equation involve only constant coefficients, they need to be rebuilt only when refinement or coarsening occurs. The decoupled solution algorithm requires to solve three linear systems at each time step. We employ a restricted additive Schwarz preconditioned GMRES method to solve the Cahn-Hilliard system and the velocity system. For the pressure Poisson equation, we use an aggregation-based algebraic multigrid preconditioned GMRES method. As far as we know, no existing combination of the above algorithms has been presented for the concerned problem.

4 Numerical experiments

The proposed algorithm is implemented using libMesh [8] for the generation of finite element stiffness matrices, and PETSc [2] for the preconditioned Krylov subspace solvers. The overall algorithm is implemented on a parallel computer with distributed memory.

In this section, we present 2D numerical experiments for a droplet travelling in a scenario when two people begin to talk face to face at $t = 0$, and an airflow is expelled horizontally from one's mouth (Γ_i: $x = 10$, $y \in [62.536, 64]$). The airflow has a parabolic profile with initial speed $V = 5$ m/s. The computational domain is $[0, 35] \times [50, 80]$ and the unit is 2.5 cm, as shown in Fig. 1. A nonuniform triangular mesh is generated such that the mesh is finer between the two people. The initial mesh has 56,568 elements and 28,285 vertices. The densities for the droplet ($\varphi = -1$) and air ($\varphi = 1$) are 10^3 kg/m^3 and 1.2 kg/m^3, the viscosities for the droplet and air are 10^{-3} Pa·s and 1.8×10^{-5} Pa·s. The interfacial tension is 0.072 N/m. The gravity constant is 9.8 m/s^2. By taking V as the characteristic velocity and the opening size of mouth 2.5 cm as the characteristic length, we obtain the following dimensionless numbers: $\lambda_\rho = 830$, $\lambda_\eta = 55$, $Re = 8333.25$, $\mathcal{B} = 707.2$, and $Fr = 10.1$. The thickness of the interface is $\epsilon = 0.002$. The static contact angle is taken as 90°. Other physical parameters are taken as in [6]. For the numerical parameters, we choose $\delta = 0.05$, $\bar{e} = 0.002$, $\gamma_c = 0.01$, $tol = 0.01$, $n_{\text{skip}} = 15$, and the time step size $\Delta t = 5 \times 10^{-4}$. For the inflow boundary condition, we consider a droplet that is ejected from Γ_i along with the airflow at $t_s = 0.05$ ms, and its initial size is determined by the ejection time δt_e, that is, $\varphi = -1$ if $x = 10, y \in [63.238, 63.298]$ and $t \in [t_s, t_s + \delta t_e]$ whereas $\varphi = 1$ on Γ_i. We consider three cases of ejection time: a. $\delta t_e = 1$ ms, b. $\delta t_e = 0.5$ ms, and c. $\delta t_e = 0.1$ ms.

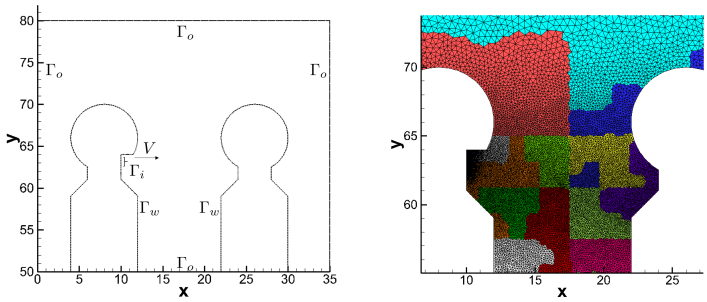

Fig. 1: (left) Computational domain and (right) a sample partition of the computational domain into 16 subdomains for the Schwarz preconditioning.

Fig. 2 shows the streamlines colored by velocity magnitude at 1.25 ms and 75 ms for case b. At the early stage, the parabolic velocity profile leads to a natural expansion of airflow. As the flow evolves, it is angled down due to the gravitational pull and generates two primary vortices, one on either side.

From Fig. 3 we see that the droplets travel ballistically subject to inertia and gravity. They overshoot the airflow stream and can reach the recipients' mucosa directly or settle on surfaces to be later picked up by the recipients. While all droplets evolve to a circle shape with the effect of surface tension, the large droplets undergo a more obvious topological change than the smaller droplets. The bottom row of the figure shows the effectiveness of the AMR method in tracking the moving

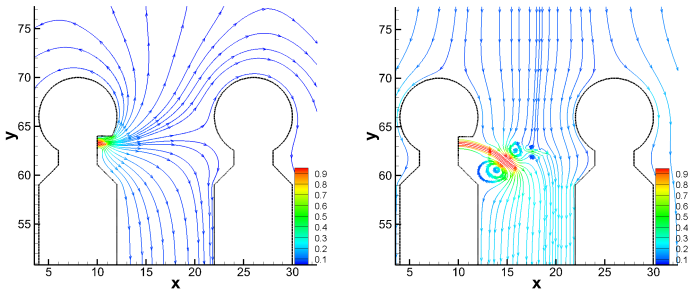

Fig. 2: Streamlines colored by velocity magnitude at (left) 1.25 ms and (right) 75 ms for case b.

interface. For these cases, usually 3 or 4 adaptive iterations are needed for each application of AMR.

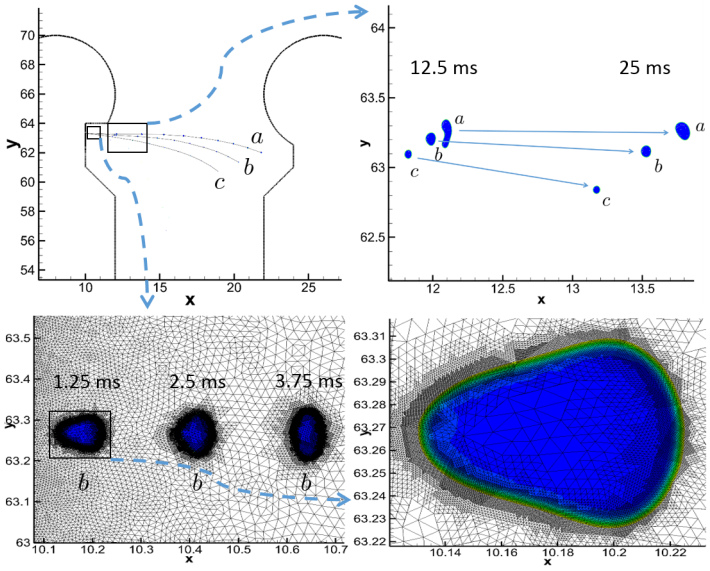

Fig. 3: (top left) Trajectory of the droplets, (top right) snapshot of droplets at 12.5 ms and 25 ms, (bottom left) adaptive mesh refinement for case *b* at 1.25 ms, 2.5 ms, and 3.75 ms, and (bottom right) enlarged view of the mesh at 1.25 ms for case b.

In the presented two-way coupling model, the airflow is affected by the motion of the droplet due to the viscosity contrast and surface tension, especially when the droplet is large. This is evidenced by the streamlines near the droplet *a* in Fig. 4 (left), one can observe a vortex street generated behind the droplet. In contrast, a smaller droplet does not influence the airflow much as shown in Fig. 4 (right).

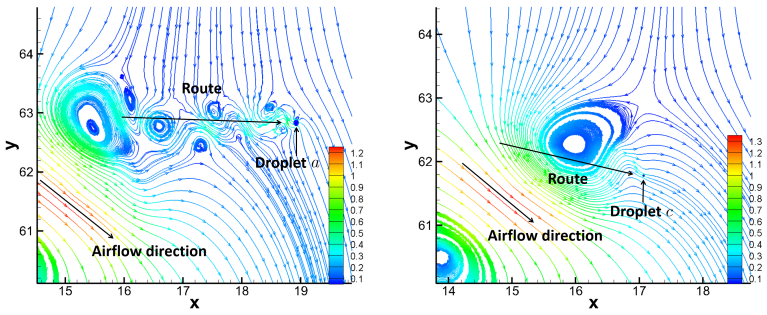

Fig. 4: Streamlines colored by velocity magnitude at 75 ms for (left) case a and (right) case c.

In Fig. 5, we show the time histories of the lift coefficient $C_l = \frac{2F_l}{\rho_1 U^2 A}$ and the drag coefficient $C_d = \frac{2F_d}{\rho_1 U^2 A}$ which evaluate the combined effect of surface tension and aerodynamic forces acting on the droplets. Here $\rho_1 = 1$, $U = 1$ are dimensionless constants. F_l, F_d, and A can be computed using the integral transformation with the surface delta function $d = \frac{1-\varphi}{2}$:

$$F_\alpha = -\frac{1}{Re}\int_\Omega \boldsymbol{\sigma} \cdot \nabla d \cdot \mathbf{e}_\alpha \mathrm{d}\Omega, \quad \text{and} \quad A = -\int_\Omega \nabla d \cdot \mathbf{n}_\varphi \mathrm{d}\Omega,$$

where $\alpha = l, d$, $\mathbf{e}_d = \mathbf{i}$, $\mathbf{e}_l = \mathbf{j}$, and $\mathbf{n}_\varphi = \frac{\nabla\varphi}{|\nabla\varphi|}$. The forces exerted on the droplets exhibit a oscillatory nature similar to the case of flow around a stationary circular cylinder, but with more irregular patterns here because of the shape dynamics of the droplets and the instability of the high Reynolds flows. The magnitude of the oscillation generally decreases as the size of the droplet becomes smaller.

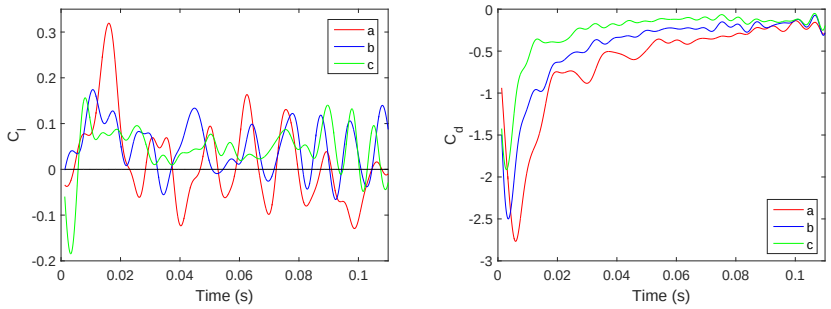

Fig. 5: Time histories of (left) lift coefficient C_l and (right) drag coefficient C_d.

5 Conclusions

We present a parallel adaptive finite element method for the modeling of a deformable droplet travelling in air. The problem is described by the Cahn-Hilliard-Navier-Stokes equations that account for the two-way coupling between the airflow and the droplet through advection and surface tension. The parallelization is realized via a Schwarz type overlapping domain decomposition method. Our results show that the size of the droplet has a significant impact on its travelling path, shape dynamics, and the ambient airflow behavior.

References

1. S. Balachandar, S. Zaleski, A. Soldati, G. Ahmadi, and L. Bourouiba. Host-to-host airborne transmission as a multiphase flow problem for science-based social distance guidelines. *Int. J. Multiph. Flow*, 132:103439, 2020.
2. S. Balay, S. Abhyankar, M. F. Adams, J. Brown, P. Brune, and K. Buschelman et al. PETSc Users Manual. Technical Report ANL-95/11-Revision 3.15, Argonne National Laboratory, 2021.
3. L. Bourouiba. The fluid dynamics of disease transmission. *Annu. Rev. Fluid Mech.*, 53:473–508, 2021.
4. C. P. Cummins, O. J. Ajayi, F. V. Mehendale, R. Gabl, and I. M. Viola. The dispersion of spherical droplets in source-sink flows and their relevance to the COVID-19 pandemic. *Phys. Fluids*, 32:083302, 2020.
5. S. Dong. An outflow boundary condition and algorithm for incompressible two-phase flows with phase field approach. *J. Comput. Phys.*, 266:47–73, 2014.
6. M. Gao and X.-P. Wang. An efficient scheme for a phase field model for the moving contact line problem with variable density and viscosity. *J. Comput. Phys.*, 272:704–718, 2014.
7. D. W. Kelly, J. P. Gago, O. C. Zienkiewicz, and I. Babuska. A posteriori error analysis and adaptive processes in the finite element method: part I error analysis. *Int. J. Numer. Methods Eng.*, 19:1593–1619, 1983.
8. B. S. Kirk, J. W. Peterson, R. H. Stogner, and G. F. Carey. `libMesh`: A C++ library for parallel adaptive mesh refinement/coarsening simulations. *Eng. Comput.*, 22:237–254, 2006.
9. V. Vuorinena, M. Aarniob, and M. Alavah et al. Modelling aerosol transport and virus exposure with numerical simulations in relation to SARS-CoV-2 transmission by inhalation indoors. *Saf. Sci.*, 130:104866, 2020.
10. M. P. Wan, G. N. S. To, C. Y. H. Chao, L. Fang, and A. Melikov. Modeling the fate of expiratory aerosols and the associated infection risk in an aircraft cabin environment. *Aerosol Sci. Technol.*, 43:322–343, 2009.